Nonlocal string order parameter in the $S = \frac{1}{2}$ Kitaev-Heisenberg ladder

Andrei Catuneanu,[1] Erik S. Sørensen,[2,*] and Hae-Young Kee[1,3,†]
[1]*Department of Physics, University of Toronto, Toronto, Ontario, Canada M5S 1A7*
[2]*Department of Physics, McMaster University, Hamilton, Ontario, Canada L8S 4M1*
[3]*Canadian Institute for Advanced Research, CIFAR Program in Quantum Materials, Toronto, Ontario, Canada M5G 1M1*

(Received 10 September 2018; published 7 May 2019)

We study the spin-$\frac{1}{2}$ Kitaev-Heisenberg (KJ) model in a two-leg ladder. Without a Heisenberg interaction, the Kitaev phase in the ladder model has Majorana fermions with local Z_2 gauge fields, and is usually described as a disordered phase without any order parameter. Here we identify a long-range nonlocal string order parameter (SOP) in the Kitaev phase which survives with a finite Heisenberg interaction. The SOP is obtained by relating the Kitaev ladder, through a nonlocal unitary transformation, to a one-dimensional XY chain with an Ising coupling to a dangling spin at every site. This differentiates the Kitaev phases from other nearby phases including a rung singlet. Two phases with nonzero SOP corresponding to ferromagnetic and antiferromagnetic Kitaev interactions are identified. The full phase diagram of the KJ ladder is determined using exact diagonalization and density matrix renormalization group methods, which shows a striking similarity to the KJ model on a two-dimensional honeycomb lattice.

DOI: 10.1103/PhysRevB.99.195112

I. INTRODUCTION

Identifying a topological order and associated phase transitions has become one of the most fascinating subjects in condensed matter physics. Exactly solvable models offering a topological order are rare, and one example is the Kitaev model described by bond-dependent interactions between nearest neighbors on a two-dimensional (2D) honeycomb lattice [1]. The exact solvability relies on the fact that the plaquette operator defined on every honeycomb plaquette commutes with the Kitaev Hamiltonian, which leads to a ground state with free Majorana fermions and gapped Z_2 vortices [1]. However, when other interactions such as the Heisenberg interaction are present, the plaquette operator no longer commutes with the Kitaev-Heisenberg (KJ) Hamiltonian, and identifying the quantity that characterizes the phase and associated phase transitions becomes a challenging task.

Taking a quasi-one-dimensional (1D) limit may give an insight into this task, because a topological phase transition can be accompanied by a nonlocal string order parameter (SOP) in 1D systems depending on the symmetry of the Hamiltonian. The best example is the spin $S = 1$ Haldane phase [2,3]. A feature of the Haldane phase is the breaking of a hidden $Z_2 \times Z_2$ symmetry revealed by a SOP defined through a nonlocal unitary transformation [4–7]. However, identifying a relevant SOP in $S = \frac{1}{2}$ ladder systems is nontrivial, particularly for highly frustrated spin interactions such as the Kitaev model, although heuristic extensions of the $S = 1$ SOP to $S = \frac{1}{2}$ ladders have been discussed [8–12].

The bond-dependent $S = \frac{1}{2}$ Kitaev ladder can be generated by taking two rows of the honeycomb lattice and connecting the dangling bonds (dashed lines in Fig. 1). A previous study [13] attempted to find a SOP on this pure isotropic Kitaev ladder, and concluded that it is a disordered phase without any SOP [13,14], while another study investigated its symmetry classification [15].

Here we study the KJ model in the two-leg ladder. We identify a long-range *nonlocal* SOP for the Kitaev phase found in the KJ model. The full phase diagram of the KJ model on the ladder is determined using the exact diagonalization (ED) and density matrix renormalization group (DMRG) techniques. A striking similarity to the 2D phase diagram on the honeycomb lattice [16] is found, despite the different geometries. The SOP differentiates the Kitaev phase from a rung singlet, and other phases corresponding to the zigzag, stripy, and ferromagnetic phases found in the 2D limit are also captured in the ladder.

II. PHASE DIAGRAM

The KJ Hamiltonian defined on a two-leg ladder is given by

$$H = K \sum_{\gamma \in \langle i,j \rangle} S_i^\gamma S_j^\gamma + J \sum_{\langle i,j \rangle} \mathbf{S}_i \cdot \mathbf{S}_j, \tag{1}$$

where $S = 1/2$, $\langle i, j \rangle$ are site indices defined on nearest-neighbor bonds, and $\gamma = x$, y, or z depending on bond type as shown in Fig. 1. The first term is the bond-dependent Kitaev interaction while the second is the isotropic Heisenberg interaction. We parametrize the spin exchanges by $K = \sin\phi$ and $J = \cos\phi$ where $\phi \in [0, 2\pi)$. When $\phi = \frac{\pi}{2}$ or $\frac{3\pi}{2}$, the Hamiltonian reduces to the Kitaev ladder studied in Ref. [13].

We first determine the entire phase diagram of the Hamiltonian as a function of ϕ. We have numerically diagonalized the KJ model using ED on a $N = 24$ site ladder using periodic boundary conditions (PBC), and DMRG. Phase boundaries were determined by identifying singular features of the second

*sorensen@mcmaster.ca
†hykee@physics.utoronto.ca

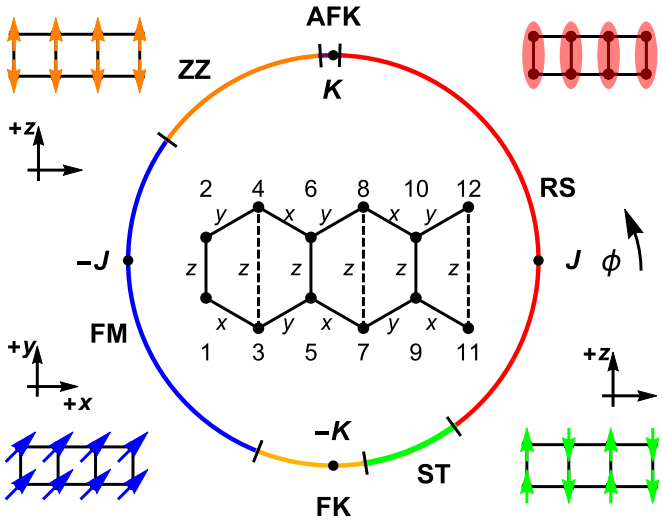

FIG. 1. Phase diagram of the KJ model as a function of ϕ with numerically determined phase boundaries labeled by black bars. Six phases are identified. The rung singlet (RS) is a singlet state, and the ZZ and ST phases have a ferromagnetic Ising ordering only along a leg and rung, respectively, shown by colored spins with accompanying quantization axes. FM has a ferromagnetic long-range order. AFK and FK are the Kitaev phases. The phase transition boundaries are similar to those of the two-dimensional (2D) KJ model. The two-leg ladder with bond definitions for the Kitaev term in Eq. (1) is depicted underneath with bond-dependent interactions denoted by x, y, and z.

derivative of the ground state energy per site, $\chi_E = -\partial_\phi^2 e_0$, the presence of a gap and the presence of a nonzero SOP. Six different phases were identified as shown in Fig. 1: (a) a rung singlet (RS) [17–19] phase, (b) an easy-plane ferromagnetic (FM) phase, (c) a phase with opposing long-range FM Ising order on each leg (ZZ), (d) a phase with alternating long-range FM Ising order on the rungs (ST), (e) antiferromagnetic Kitaev (AFK) phase, and (f) FM Kitaev (FK) phase. With the exception of the FM phase, which is gapless and extensively degenerate, all of the phases are gapped and their nature have been explored [20–22].

The AF and FM Heisenberg limits at $\phi = 0$ and π are located in the RS and FM phases (black dots in Fig. 1). In the thermodynamic limit, the ZZ, ST, AFK, and FK phases all have twofold degenerate ground state while the RS phase has a unique ground state. We estimate the other transitions as: RS-AFK: $\phi \simeq 0.487\pi$, AFK-ZZ: $\phi \simeq 0.53\pi$, ZZ-FM: $\phi \simeq 0.81\pi$, FM-FK: $\phi \simeq 1.377\pi$, FK-ST: $\phi \simeq 1.562\pi$, and ST-RS: $\phi \simeq 1.71$. Despite the manifestly 1D nature of the ladder geometry, the phase diagram is strikingly similar to that of the 2D 24-site honeycomb ED phase diagram for the KJ model [20–22] and we have chosen the naming of the ZZ and ST magnetically ordered phases to correspond. The only qualitative difference though is that at the AFK to ZZ transition no feature is observed in χ_E nor in the fidelity susceptibility in the ladder, implying that the transition is likely high order with $2/\nu - d < 0$ [23] or $\nu > 2$, which is different from the 2D honeycomb. A level crossing between the two ground states, split by finite-size effects, is however observed at $\phi \simeq 0.515\pi$. A further discussion on this transition is presented in the Supplemental Material (SM) [24].

Let us first focus on the nature of Kitaev phases near $\phi = \frac{\pi}{2}$ and $\frac{3\pi}{2}$. The ground states of the ladder at the Kitaev points, with $\pm K$, have been described as disordered without a SOP [13,14]. Here we demonstrate the existence of a long-range SOP in both AFK and FK phases with and without Heisenberg interaction. We shall do this by explicitly establishing a *nonlocal* unitary transformation V that maps H to another Hamiltonian with a nonzero *local* order parameter. Applying the inverse transformation to this local order parameter then yields the (hidden) SOP in the original model. As we shall demonstrate, this SOP differentiates the Kitaev phases from neighboring phases.

III. THE UNITARY OPERATOR V

Previous studies [5–7] have exclusively considered $S = 1$ models for the technical reason that the integer spin identity $\exp(2i\pi S_j^x S_k^z) = I$ is not satisfied for $S = \frac{1}{2}$. However, even without this identity we can still define a suitable unitary operator for the Kitaev ladder. In order to define such a unitary operator, we group the $S = \frac{1}{2}$ spins in pairs. We make the simple choice to group spins on the rungs of the ladder. Following the numbering convention of the lattice sites shown in Fig. 1 we then define the following nonlocal unitary operator for a N-site ladder with open boundary conditions (OBC):

$$V = \prod_{\substack{j+1<k \\ j \text{ odd},\ k \text{ odd} \\ j=1,\ldots,N-3 \\ k=3,\ldots,N-1}} U(j,k), \tag{2}$$

where the individual $U(j,k)$ is given as follows: $U(j,k) = e^{i\pi(S_j^y + S_{j+1}^y)(S_k^x + S_{k+1}^x)}$. Clearly all $U(j,k)$ and V are unitary; and, as mentioned above, $j, j+1$ and $k, k+1$ group the $S = \frac{1}{2}$ spins on a rung. We note that $[U(j,k), U(l,m)] = 0 \ \ \forall\ j,k,l,m$ which allows us to rearrange terms in a convenient manner.

Under the unitary transformation V, S_i^α will transform in a way that depends on i as shown in the SM [24]. Note that V effectively *moves* the bond and changes the sign of the interaction as sketched in Fig. 2(a). Using the numbering of the sites as in Fig. 1, the interactions around a plaquette transform under V as follows:

$$\begin{aligned} V S_{2n+1}^x S_{2n+3}^x V^{-1} &= -S_{2n+1}^x S_{2n+4}^x, \\ V S_{2n+2}^x S_{2n+4}^x V^{-1} &= -S_{2n+2}^x S_{2n+3}^x, \end{aligned} \tag{3}$$

with $n = 0, 1, 2, \ldots$. For the y-y interaction, it changes to

$$\begin{aligned} V S_{2n+1}^y S_{2n+3}^y V^{-1} &= -S_{2n+2}^y S_{2n+3}^y, \\ V S_{2n+2}^y S_{2n+4}^y V^{-1} &= -S_{2n+1}^y S_{2n+4}^y. \end{aligned} \tag{4}$$

On the other hand, the z-z interaction on the rungs, i.e., $S_i^z S_{i+1}^z$ for $i = 1, 3, 5, \ldots$, is unchanged. Other transformations of interaction terms are given in the SM [24].

With these transformations the original Kitaev Hamiltonian in Eq. (1) (with $J = 0$ and OBC) is transformed as

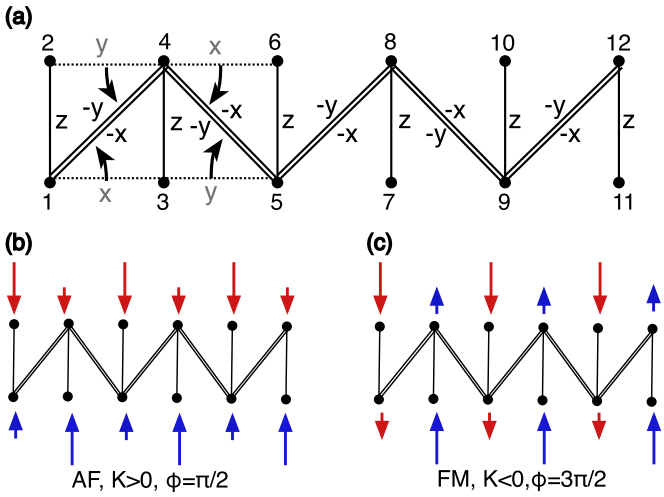

FIG. 2. (a) The movement of bonds by the unitary operator V is indicated in the first part of the chain. Schematic view of (b) the ordering at the AF Kitaev point $\phi = \frac{\pi}{2}$, and (c) the FM Kitaev point $\phi = \frac{3\pi}{2}$ for the H_{d-Z}. In each case one of two degenerate ground states is shown, with the other one obtained by interchanging up and down spins on the dangling spin sites. The red/blue coloring represents the S^z components of the spin, up/down, at each site. Large arrows at the dangling sites are $\pm 1/2$.

$VHV^{-1} = H_{d-Z}$ with

$$H_{d-Z} = K \sum_{n=0} \tilde{S}^z_{2n+1}\tilde{S}^z_{2n+2} - K \sum_{n,\alpha=x,y} \left(\tilde{S}^\alpha_{4n+1}\tilde{S}^\alpha_{4n+4} + \tilde{S}^\alpha_{4n+4}\tilde{S}^\alpha_{4n+5}\right), \quad (5)$$

where $\tilde{S}$ denotes the spins in H_{d-Z}. The transformed Hamiltonian is essentially an XY chain with Ising coupling to a dangling spin at every site, which we therefore name the "dangling-Z" model.

H_{d-Z} has several interesting properties, most importantly, all the "dangling" $\tilde{S}^z$ commute with H_{d-Z}. With our numbering:

$$\left[\tilde{S}^z_{4n+2}, H_{d-Z}\right] = 0, \quad \left[\tilde{S}^z_{4n+3}, H_{d-Z}\right] = 0, \quad (6)$$

for all integers $n \geqslant 0$. Hence, each eigenstate of H_{d-Z} will be part of a $2^{N/2}$ manifold of states generated by the different configurations of the free $\tilde{S}^z$ spins. All $2^{N/2}$ states are twofold degenerate, corresponding to flipping all the dangling spins. Sketches of one of the two ground states at the Kitaev points with the dangling-Z spins fully polarized are shown in Figs. 2(b) and 2(c). Following Kitaev's idea, one can represent H_{d-Z} in terms of Majorana operators.

H_{d-Z} can be mapped to free Majorana fermions along the deformed zigzag chain which couple to a Z_2 flux at dangling sites via the $\tilde{S}^z\tilde{S}^z$ interaction as shown in the SM [24].

Thus the $2^{N/2}$ manifold of states can be understood in terms of Z_2 flux degrees of freedom.

IV. STRING ORDER PARAMETER

With the dangling spin integrals of motion, H_{d-Z} can have long-range order in the sense that $\lim_{r\to\infty}\langle \tilde{S}^\alpha_i \tilde{S}^\alpha_{i+r}\rangle \neq 0$, $\alpha = x, y, z$. We can then define string correlation functions in the original H, Eq. (1), that are ordinary correlation functions in the transformed Hamiltonian H_{d-Z}. We define a z-string correlation function starting from the leftmost dangling site 2:

$$\langle O^z(r)\rangle = 4\left\langle \tilde{S}^z_2 \tilde{S}^z_{2+r}\right\rangle = (-1)^{\lfloor (r+1)/2\rfloor} \times \begin{cases} \left\langle \sigma^y_1 \sigma^x_2 \left(\prod_{k=3}^{r+1} \sigma^z_k\right)\sigma^x_{2+r}\sigma^y_{3+r}\right\rangle & r \text{ even}, \\ \left\langle \sigma^y_1 \sigma^x_2 \left(\prod_{k=3}^{r+1} \sigma^z_k\right)\sigma^y_{2+r}\sigma^x_{3+r}\right\rangle & r \text{ odd}, \end{cases} \quad (7)$$

where σ_i are the Pauli matrices in the original H. Note that $O^z(r)$ contains a combination of x, y, z Pauli matrices. With this definition, long-range order in $\langle \tilde{S}^z_i \tilde{S}^z_{i+r}\rangle$ results in long-range order in $O^z(r)$. Similarly, an x-string operator that starts in the leftmost site 1 is found:

$$\langle O^x(r)\rangle = 4\left\langle \tilde{S}^x_1 \tilde{S}^x_{1+r}\right\rangle = (-1)^{\lfloor (r+1)/2\rfloor} \times \begin{cases} \left\langle \sigma^x_1 \left(\prod_{k=3}^{r-1} \sigma^x_k\right)\sigma^x_r\right\rangle & r \text{ odd}, \\ \left\langle \sigma^x_1 \left(\prod_{k=3}^{r} \sigma^x_k\right)\sigma^x_{r+2}\right\rangle & r \text{ even}, \end{cases} \quad (8)$$

with a similar expression for the y-string operator. Note that in this case the string of σ^x's is not consecutive.

$O^z(r)$ is clearly long ranged at the Kitaev points, $\phi = \pi/2$ and $3\pi/2$, because of the dangling $\tilde{S}^z$ local integrals of motion. However, in the presence of a nonzero Heisenberg term J, new terms arise in VHV^{-1} (see the SM [24]) which is no longer simply equal to Eq. (5). It is therefore not at all obvious that $O^z(r)$ will show long-range order. To understand the hidden order near the Kitaev points with $J \neq 0$, we define an associated string order parameter as follows:

$$O^z = \sqrt{|O^z(3L/4)|_{\max}}, \quad (9)$$

where $|O^z(3L/4)|_{\max}$ refers to the maximal value $O^z(r)$ takes in the neighborhood of $r = 3L/4$. This definition avoids effects from the open boundary at $r = L$. With this definition of an SOP, we now map out the phase around $\phi = \pi/2$ and $\phi = 3\pi/2$ where the "hidden" order associated with the z-string correlation functions $O^z(r)$ is present. On the other hand, the x- and y-string correlation functions $O^{x/y}(r)$ show exponentially decaying behavior at the Kitaev points, $O^{x/y}(r) = ae^{-r/\xi}$ with $\xi \sim 4$ and $O^{x/y}$ is not long ranged in the FK and AFK phases although it is trivially long range in the FM phase where instead O^z is zero.

Numerical results for $\langle O^z\rangle$ as well as the gaps ΔE_1 and ΔE_2 to the first and second excited states are shown near the AFK and FK phases in Fig. 3. Clearly $\langle O^z(r)\rangle$ attains the extremal values of ± 1 in both cases exactly at the Kitaev points even though we have verified that all usual spin-spin correlators are *extremely* short range. Here $\langle O^z\rangle$ is obtained from the $\langle \tilde{S}^z_2 \tilde{S}^z_{2+r}\rangle$ correlation function but we have checked that using $\langle \tilde{S}^z_{N/2} \tilde{S}^z_{N/2+r}\rangle$ only makes minor changes. In the $N \to \infty$ limit the SOP remain finite in the FK and AFK phases with ΔE_1 and ΔE_2 disappearing at the quantum critical points.

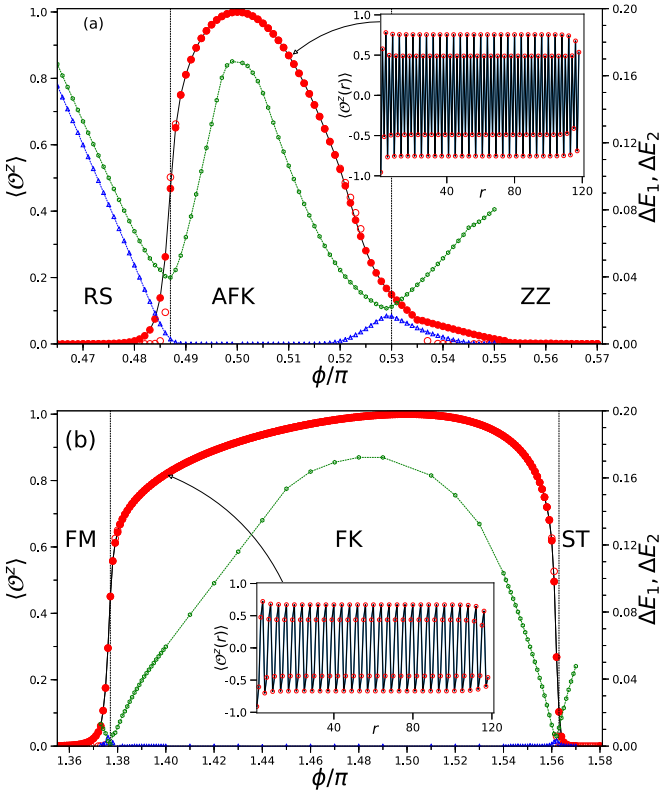

FIG. 3. $\langle O^z \rangle$ determined from DMRG calculations on a ladder with $N = 120/400$ sites (solid/open red circles) and OBC with a typical truncation error of 10^{-11}. (a) Near the AFK [inset for $\langle O^z(r) \rangle$ vs r at $\phi = 0.51\pi$], and (b) near the FK [inset for $\langle O^z(r) \rangle$ vs r at $\phi = 1.40\pi$]. The energy gap to the first excited state ΔE_1 and the second excited state ΔE_2 are shown by blue triangles and green circles, respectively. Both gaps are determined by DMRG calculations with $N = 60$ and PBC with a typical truncation error of 10^{-9} (10^{-6}) on the ground (excited) state.

V. ENTANGLEMENT SPECTRUM

A topological phase is characterized by a double degeneracy of the entire entanglement spectrum (ES) [25,26] obtained from the Schmidt coefficients λ_α of the partition. Indeed the ES spectrum shown in Fig. 4 is doubly degenerate for both AFK and FK, and RS when partitioned with one middle-rung cut as shown in the 12-site ED with open boundary conditions (Fig. 9 in the SM [24]). The middle-rung cut is important to generate the double degeneracy of the entire ES because a pairing term of Majorana fermions occurs via the dangling sites in H_{d-Z} as shown in the SM [24].

Thus, without the middle-rung cut, the degeneracy is not expected. We have indeed confirmed that a vertical cut, not involving the middle-rung cut, does not give the ES degeneracy.

The transition between the FK and ST/FM as well as the AFK-ZZ transition is signaled by the disappearance of the double degeneracy present in the FK. However, with our cut the RS-AFK transition is between two phases *both* with doubled ES that can only be differentiated by the SOP. It is also important to differentiate the different natures of RS and AFK/FK. The edge states of RS are $S = \frac{1}{2}$, as they appear

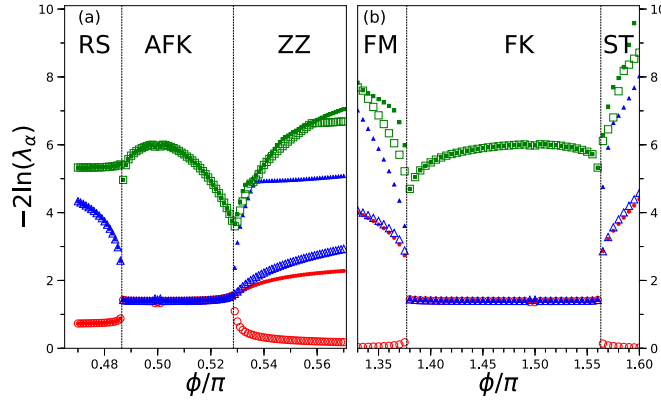

FIG. 4. Entanglement spectrum (ES) partitioned with a cut of one middle rung is shown around (a) the AFK and (b) FK phases with iDMRG and OBC. Open and filled red circles, open and filled blue triangles, and open and filled green squares correspond to the first to sixth eigenvalues, respectively. See the main text for implications of the ES results.

when a singlet formed on the middle rung is cut, while the edge states of AFK/FK are Majorana fermions. They are fractionalized excitations of $S = \frac{1}{2}$, similar to the original Kitaev honeycomb model.

The ES flow at the AFK-ZZ phase is rather unusual. Instead of a discrete jump in the ES spectrum at the AFK-ZZ transition, a smooth splitting of the fourfold degenerate lowest level is observed, indicative of a high order transition. A further study is required to fully understand the nature of the AFK-ZZ transition.

VI. SUMMARY AND DISCUSSION

We identified a nonlocal SOP in the KJ ladder model, which is a unique quantity that characterizes a topological phase. This SOP is nonzero in the AFK and FK phases of the KJ ladder, differentiating them from other nearby phases. We note that the short-range string $\langle O^z(r = 4) \rangle = \langle W_p \rangle$, where the plaquette operator $W_p = \sigma_1^y \sigma_2^x \sigma_3^z \sigma_4^z \sigma_5^x \sigma_6^y$ and the subscripts 1–6 refer to the consecutive sites on a hexagon shown in Fig. 1. This implies that the plaquette expectation value is insufficient to capture the Kitaev phase when the Heisenberg term is present. Thus, the *long-range* SOP is essential to characterize the Kitaev phases of the KJ ladder. Furthermore, the transition boundaries surrounding the AFK and FK phases are strikingly close to those of the 2D 24-site honeycomb ED result [16], suggesting that the transitions are determined by the closing of the Z_2 vision gap.

The ladder ZZ, ST, and RS phases develop a local magnetic order parameter in the 2D limit. On the other hand, the AFK and FK phases become the Kitaev spin liquid in the 2D limit, and one may expect long-range entanglement to develop only in the true 2D limit. Such development of long-range entanglement starting from the Kitaev phase of the ladder with its characteristic SOP to the 2D Kitaev spin liquid is a particularly interesting question for a future study. Additionally, further studies on the Kitaev model including other interactions and/or magnetic field using the ladder geometry will advance our understanding of Kitaev materials [27–31].

ACKNOWLEDGMENTS

This research was supported by NSERC and CIFAR. Computations were performed in part on the GPC and Niagara supercomputers at the SciNet HPC Consortium. SciNet is funded by: the Canada Foundation for Innovation under the auspices of Compute Canada; the Government of Ontario; Ontario Research Fund - Research Excellence; and the University of Toronto. Computations were also performed in part by support provided by SHARCNET (www.sharcnet.ca) and Compute/Calcul Canada (www.computecanada.ca). Part of the numerical calculations were performed using the ITensor library (http://itensor.org) typically with a precision of 10^{-11} and truncation errors not exceeding 10^{-9} for the ground state and 10^{-6} for excited states.

[1] A. Kitaev, Ann. Phys. **321**, 2 (2006).
[2] F. D. M. Haldane, Phys. Lett. A **93**, 464 (1983).
[3] F. D. M. Haldane, Phys. Rev. Lett. **50**, 1153 (1983).
[4] M. den Nijs and K. Rommelse, Phys. Rev. B **40**, 4709 (1989).
[5] T. Kennedy and H. Tasaki, Commun. Math. Phys. **147**, 431 (1992).
[6] T. Kennedy and H. Tasaki, Phys. Rev. B **45**, 304 (1992).
[7] M. Oshikawa, J. Phys.: Condens. Matter **4**, 7469 (1992).
[8] S. R. White, Phys. Rev. B **53**, 52 (1996).
[9] Y. Nishiyama, N. Hatano, and M. Suzuki, J. Phys. Soc. Jpn. Suppl. **65**, 560 (1996).
[10] E. H. Kim, G. Fath, J. Sólyom, and D. J. Scalapino, Phys. Rev. B **62**, 14965 (2000).
[11] G. Fath, Ö. Legeza, and J. Sólyom, Phys. Rev. B **63**, 134403 (2001).
[12] F. Anfuso and A. Rosch, Phys. Rev. B **76**, 085124 (2007).
[13] X.-Y. Feng, G.-M. Zhang, and T. Xiang, Phys. Rev. Lett. **98**, 087204 (2007).
[14] E. Barouch and B. M. McCoy, Phys. Rev. A **3**, 786 (1971).
[15] R. Haghshenas, A. Langari, and A. T. Rezakhani, J. Phys.: Condens. Matter **28**, 176001 (2016).
[16] J. Chaloupka, G. Jackeli, and G. Khaliullin, Phys. Rev. Lett. **110**, 097204 (2013).
[17] E. Dagotto, J. Riera, and D. Scalapino, Phys. Rev. B **45**, 5744 (1992).
[18] T. Barnes, E. Dagotto, J. Riera, and E. S. Swanson, Phys. Rev. B **47**, 3196 (1993).
[19] S. R. White, R. M. Noack, and D. J. Scalapino, Phys. Rev. Lett. **73**, 886 (1994).
[20] J. Chaloupka, G. Jackeli, and G. Khaliullin, Phys. Rev. Lett. **105**, 027204 (2010).
[21] D. Gotfryd, J. Rusnačko, K. Wohlfeld, G. Jackeli, J. Chaloupka, and A. M. Oleś, Phys. Rev. B **95**, 024426 (2017).
[22] C. E. Agrapidis, J. van den Brink, and S. Nishimoto, Sci. Rep. **8**, 1815 (2018).
[23] A. F. Albuquerque, F. Alet, C. Sire, and S. Capponi, Phys. Rev. B **81**, 064418 (2010).
[24] See Supplemental Material at http://link.aps.org/supplemental/10.1103/PhysRevB.99.195112 for further details.
[25] H. Li and F. D. M. Haldane, Phys. Rev. Lett. **101**, 010504 (2008).
[26] F. Pollmann, E. Berg, A. M. Turner, and M. Oshikawa, Phys. Rev. B **85**, 075125 (2012).
[27] W. Witczak-Krempa, G. Chen, Y. B. Kim, and L. Balents, Ann. Rev. Condens. Matter Phys. **5**, 57 (2014).
[28] J. G. Rau, E. K.-H. Lee, and H.-Y. Kee, Ann. Rev. Condens. Matter Phys. **7**, 195 (2016).
[29] S. Trebst, arXiv:1701.07056.
[30] M. Hermanns, I. Kimchi, and J. Knolle, Ann. Rev. Condens. Matter Phys. **9**, 17 (2018).
[31] S. M. Winter, A. A. Tsirlin, M. Daghofer, J. van den Brink, Y. Singh, P. Gegenwart, and R. Valentí, J. Phys.: Condens. Matter **29**, 493002 (2017).